Image denoising using regularized Butterworth wavelet frames

Amir Z. Averbuch Valery A. Zheludev
School of Computer Science
Tel Aviv University
Tel Aviv 69978, Israel

January 31, 2008

Abstract

We present an efficient algorithm for image restoration from highly noised originals. The algorithm is based on diverse library of tight and semi-tight wavelet frames. Unlike majority of current denoising methods, which threshold the transform coefficients, our algorithm performs direct and inverse multiscale transforms using properly modified frame filters. No thresholding is applied. The processing is linear. The algorithm is fast and can be implemented in real time. It depends on one numerical parameter, which is estimated from the noise level.

1 Introduction

Denoising is one of ever-actual problems in image processing. Usually, the structure of an image is distorted by different types of noise. The goal of denoising process is to reveal the essential structure of the image, without producing of artifacts. Currently, common approach consists in application of a multiscale transform to the image. This is followed by manipulation of the transform coefficients. Typically, a wavelet transform is applied and the coefficients are thresholded or shrunk (soft thresholding) according to a strategy that is usually based on statistical modeling of the wavelet coefficients from different scales. The VisuShrink, SureShrink and Bayesian schemes of shrinkage of wavelet coefficients ([5, 4, 13, 6, 11]) provide good results when the noise level is moderate. Better results are reported when the interscale dependency of the wavelet coefficients is taken into account ([12]). Denoising performance is improved when overcomplete expansions of images such as non-decimated wavelet transforms [3, 9] or wavelet frame transforms [8] are applied rather than the standard wavelet transforms. However, when the noise becomes strong, the performance of the schemes, which are based on thresholding, becomes degraded. Discarding high number of the transform coefficients either results in oversmoothing the image or in producing miltiple artifacts. One of the best denoising results was obtained by Scale Mixtures of Gaussians (GSM) method presented in [7]. There, the steerable

pyramides transform ([14]) was applied to the image. Then, a sophisticated statistical estimation of the transform coefficients, which is based on GSM, is carried out. The inverse transform is applied to the estimated coefficients. The peak signal-to noise ratio (PSNR) results in [7] are impressive but, regretfully, images that were restored from strongly noised originals have distortions with non-desired artifacts. A couple of GSM-denoised images are displayed in Section 4. A drawback of the GSM algorithm is its high computational cost. Therefore, processing of an 256×256 image takes 40 seconds in MATLAB implementation.

In this paper, we present a new denoising method, which is based on the application of the regularized Butterworth wavelet frame transforms to noisy images. A family of interpolatory wavelet frames in the space of infinite discrete-time signals belonging to the space l_1 was presented in [2]. These frames, which are related to Butterworth filters, were derived from discrete splines. This family contains framelets with different number of vanishing moments, which can be arbitrarily high. The filtering in [2] was implemented in a recursive mode. In this paper, we modify this construction in order to use the discrete Fourier transform (DFT). This modification adds a flexibility to the implementation and enables to regularize the transforms without an increase of its computational cost.

The idea behind the regularization is the following. The application of the high- and low-pass filters reduce the numerical differentiation by different orders. Typically, this operation enhances the noise level. We modify these filters using a method that is based on Tikhonov regularization [15]. The denoising procedure consists of subsequent application of the direct and inverse regularized multiscale framelet transforms. No thresholding is applied. Thus, processing is linear. We achieve significant noise suppression while retaining the coherent structure of the signal without producing artifacts. This method proved to be especially efficient in processing images that are corrupted by a very strong noise, sometimes with negative PSNR. While the GSM method produces better PSNR than ours, our method neither distorts the structures of the images nor produces artifacts even in the presence of strong noise. In addition, processing of an 512×512 image takes 1.2 seconds in MATLAB implementation. The algorithm can work in real-time. The extension of the method to higher dimensions with a reasonable computational cost is straightforward.

The paper is organized as follows. In Section 2, we describe the design of the Butterworth wavelet frames for spaces of periodic signals. We explain how to derive interpolatory tight and semi-tight frames from filter banks, consisting of one low-pass, one band-pass and one high-pass filter. We construct a multitude of frames using filters that are related to the Butterworth filters. We introduce a notion of quasi-vanishing moments (QWM), which is a substitute for the notion of vanishing moments for the space of periodic signals. In Section 3 we discuss why wavelet frames are good for denoising and present the regularization of the Butterworth frames. In Section 4, we show how to implement the framelet transforms of images and demonstrate the results by the application of regularized filter

banks to denoising of a few benchmark images that were contaminated by strong noise. The results are compared to results that are obtained from the GSM technuque. The GSM images were downloaded from the web site of E. Simoncelli http://www.cns.nyu.edu/∼eero/.

2 Butterworth wavelet frames

In this section, we briefly outline the construction of Butterworth wavelet frames. Unlike [2], we operate on signals, which are $N = 2^j$-periodic, using the discrete Fourier transform (DFT) rather than the z-transform. The space of such signals is denoted by $\mathfrak{S}^j$.

2.1 Preliminaries

Let j be an integer number. Throughout the paper we assume $N = 2^j$ and $\cdot_k^j$ stands for $\cdot_{k=0}^{2^j-1}$. Denote $\omega \triangleq e^{2\pi \mathrm{i}/N}$. Then, the DFT of a signal $\mathbf{x} \triangleq \{x(k)\}_k^j$ and its inverse $\widehat{\mathbf{x}} \triangleq \{\hat{x}(n)\}_n^j$ are

$$\hat{x}(n) = \sum_k^j \omega^{-kn} x(k), \quad x(k) = \frac{1}{N} \sum_n^j \omega^{kn} \hat{x}(n).$$

The inner product of the two signals is

$$\langle \mathbf{x}, \mathbf{y} \rangle \triangleq \sum_k^j x(k)\, y(k) = \frac{1}{N} \sum_n^j \hat{x}(n) \hat{y}(-n), \quad \|\mathbf{x}\| \triangleq \sqrt{\langle \mathbf{x}, \mathbf{x} \rangle}.$$

Filtering the signal $\mathbf{x}$ with a filter $\mathbf{H} \triangleq \{H(k)\}_{k=-\infty}^{\infty}$ (which also belongs to $\mathfrak{S}^j$) is the cyclic discrete convolution

$$\mathbf{y} = \mathbf{H} \star \mathbf{x} \Longleftrightarrow y(k) = \sum_l^j H(k-l) x(l), \quad \hat{y}(n) = \hat{H}(n)\, \hat{x}(n), \quad k, n = 0, \ldots, N-1. \tag{2.1}$$

If filtering a signal is accompanied by downsampling or upsampling then it is called multirate filtering. For example, application of the time-reversed filter $\tilde{\mathbf{H}}$ followed by downsampling with factor of 2 to the signal $\mathbf{x} \in \mathfrak{S}^j$ is

$$\tilde{y}(k) = \sum_l^j \tilde{H}(l - 2k)\, x(l), \quad k = 0, \ldots, N/2 - 1. \tag{2.2}$$

Application of the filter $\mathbf{H}$ to the signal $\tilde{\mathbf{y}} \triangleq \{\tilde{y}(k)\}_k^{j-1} \in \mathfrak{S}^{j-1}$, which is upsampled by factor 2, is

$$\xi(k) = \sum_l^{j-1} H(k - 2l)\, \tilde{y}(l) \Longleftrightarrow \hat{\xi}(n) = \hat{H}(n) \hat{\tilde{y}}(n), \quad k, n = 0, \ldots, N-1. \tag{2.3}$$

Polyphase representation. Let $\mathbf{q} \stackrel{\Delta}{=} \{q(k)\} \in \mathfrak{S}^j$. We denote by $\mathbf{q^e}$ and $\mathbf{q^o}$ its even and odd components, respectively:

$$\mathbf{q^e} \stackrel{\Delta}{=} \{q(2k)\}\,,\ \mathbf{q^o} \stackrel{\Delta}{=} \{q(2k+1)\}\,, \quad \widehat{q^e}(n) = \sum_k^{j-1} \omega^{-2kn} q(2k),\ \widehat{q^o}(n) = \sum_k^{j-1} \omega^{-2kn} q(2k+1).$$

Then,

$$\widehat{q}(n) = \widehat{q^e}(2n) + \omega^{-n}\widehat{q^o}(2n) \tag{2.4}$$

is the polyphase representation of the signal $\mathbf{q}$. Filtering can be represented in a polyphase mode. When the time-reversed filter $\tilde{\mathbf{H}}$ is applied to the signal $\mathbf{x}$ by $\hat{y}(n) = \hat{\tilde{H}}(-n)\,\hat{x}(n)$, then, the polyphase components are

$$\widehat{y^e}(n) = \widehat{\widetilde{H^e}}(-n)\,\widehat{x^e}(n) + \widehat{\widetilde{H^o}}(-n)\,\widehat{x^o}(n),\ \widehat{y^o}(n) = \widehat{\widetilde{H^o}}(-n)\,\hat{x}^e(n) + \omega^{2n}\widehat{\widetilde{H^e}}(-n)\,\hat{x}^o(n).$$

If filtering is followed by downsampling as in Eq. (2.2), then only the even polyphase component is retained:

$$\widehat{\tilde{y}}(n) = \widehat{\widetilde{H^e}}(-n)\,\widehat{x^e}(n) + \widehat{\widetilde{H^o}}(-n)\,\widehat{x^o}(n). \tag{2.5}$$

If filtering is applied to the upsampled signal $\tilde{\mathbf{y}}$ as in Eq. (2.3) then the polyphase components of the output are

$$\widehat{x^e}(n) = \widehat{H^e}(n)\widehat{\tilde{y}}(n), \quad \widehat{x^o}(n) = \widehat{H^o}(n)\widehat{\tilde{y}}(n). \tag{2.6}$$

In this paper, we consider 3-channel filter banks, where each contains one low-pass, one band-pass and one high-pass filters and the downsampling/upsampling factor is 2. The analysis filter bank $\widetilde{\mathbf{F}}$ is formed by the filters $\widetilde{\mathbf{H}}_L$, $\widetilde{\mathbf{H}}_B$ and $\widetilde{\mathbf{H}}_H$, respectively. Reverse application of these filters to a signal $\mathbf{x} \in \mathfrak{S}^j$ is followed by downsampling

$$\tilde{y}_{L/B/H}(k) = \sum_l^j \tilde{H}_{L/B/H}(l-2k)\,x(l), \quad k = 0, \ldots, N/2-1. \tag{2.7}$$

The output from the analysis filter bank are the signals $\tilde{\mathbf{y}}_{L/B/H}(k) \in \mathfrak{S}^{j-1}$. The synthesis filter bank $\mathbf{F}$, which is applied to the upsampled signals from $\mathfrak{S}^{j-1}$, is formed by the filters $\mathbf{H}_L$, $\mathbf{H}_B$ and $\mathbf{H}_H$, respectively. Subsequent application of the analysis filter bank $\widetilde{\mathbf{F}}$ and the synthesis filter bank $\mathbf{F}$ to a signal $\mathbf{x} \in \mathfrak{S}^j$ reproduces this signal in the following way

$$x(k) = \sum_l^{j-1} H_L(k-2l)\,\tilde{y}_L(l) + H_B(k-2l)\,\tilde{y}_B(l) + H_H(k-2l)\,\tilde{y}_H(l). \tag{2.8}$$

Then, the pair $\left\{\widetilde{\mathbf{F}}, \mathbf{F}\right\}$ constitutes a perfect reconstruction filter bank (PRFB).

Application of the PRFB can be expressed via operations with the polyphase matrices:

$$\begin{pmatrix} \widehat{\tilde{y}}_L(n) \\ \widehat{\tilde{y}}_B(n) \\ \widehat{\tilde{y}}_H(n) \end{pmatrix} = \widetilde{\mathbf{P}}(-n) \cdot \begin{pmatrix} \widehat{x^e}(n) \\ \widehat{x^o}(n) \end{pmatrix}, \quad \begin{pmatrix} \widehat{x^e}(n) \\ \widehat{x^o}(n) \end{pmatrix} = \mathbf{P}(n) \cdot \begin{pmatrix} \widehat{\tilde{y}}_L(n) \\ \widehat{\tilde{y}}_B(n) \\ \widehat{\tilde{y}}_H(n) \end{pmatrix},\ n = 0, \ldots, \frac{N}{2} - 1, \tag{2.9}$$

where

$$\widetilde{\mathbf{P}}(n) \triangleq \begin{pmatrix} \widehat{\widetilde{H}}_L^e(n) & \widehat{\widetilde{H}}_L^o(n) \\ \widehat{\widetilde{H}}_B^e(n) & \widehat{\widetilde{H}}_B^o(n) \\ \widehat{\widetilde{H}}_H^e(n) & \widehat{\widetilde{H}}_H^o(n) \end{pmatrix}, \quad \mathbf{P}(n) \triangleq \begin{pmatrix} \widehat{H}_L^e(n) & \widehat{H}_B^e(n) & \widehat{H}_H^e(n) \\ \widehat{H}_L^o(n) & \widehat{H}_B^o(n) & \widehat{H}_H^o(n) \end{pmatrix}, \; n = 0, \ldots, \frac{N}{2} - 1 \quad (2.10)$$

are the analysis and the synthesis polyphase matrices, respectively.

Therefore, the perfect reconstruction property is represented by

$$\mathbf{P}(n) \cdot \widetilde{\mathbf{P}}(-n) = \begin{pmatrix} 1 & 0 \\ 0 & 1 \end{pmatrix}, \; n = 0, \ldots, \frac{N}{2} - 1. \quad (2.11)$$

2.2 Frames generated by filter banks

Perfect reconstruction filter banks form frames in the signal space $\mathfrak{S}^j$.

Definition 2.1 *The system $\tilde{\Phi} \triangleq \{\tilde{\phi}(k)\} \in \mathfrak{S}^j$ of signals forms a frame in the signal space $\mathfrak{S}^j$ if there exist positive constants A and B such that for any signal $\mathbf{x} \in \mathfrak{S}^{\mathbf{j}}$*

$$A\|\mathbf{x}\|^{\mathbf{2}} \le \sum_{\mathbf{k}}^{\mathbf{j}} |\langle \mathbf{x}, \tilde{\phi}(\mathbf{k}) \rangle|^{\mathbf{2}} \le \mathbf{B}\|\mathbf{x}\|^{\mathbf{2}}.$$

If the frame bounds A and B are equal to each other then the frame is called tight.

If the system $\tilde{\Phi}$ is a frame then there exists another frame $\Phi \triangleq \{\phi(k)\}$ in the signals space such that any signal $\mathbf{x}$ can be expanded into the sum $\mathbf{x} = \sum_{\mathbf{k}} \langle \mathbf{x}, \tilde{\phi}(\mathbf{k}) \rangle \, \phi(\mathbf{k})$. The analysis $\tilde{\Phi}$ and synthesis Φ frames can be interchanged. Together they form the so-called bi-frame. If the frame is tight then Φ can be chosen to be $\Phi = c\tilde{\Phi}$.

If the number of elements $\{\tilde{\phi}(k)\}$ of the analysis frame $\tilde{\Phi}$ is equal to N then the synthesis frame Φ is unique and the frames $\tilde{\Phi}$ and Φ form a biorthogonal pair of bases for the signal space $\mathfrak{S}^j$.

Assume that the pair $\left\{\widetilde{\mathbf{F}}, \mathbf{F}\right\}$, which was described above, constitutes the PRFB. We define the discrete-time framelets of the first scale as the impulse responses of the corresponding filters:

$$\tilde{\varphi}^1_{L/B/H}(k) \triangleq \tilde{H}_{L/B/H}(k), \quad \varphi^1_{L/B/H}(k) \triangleq H_{L/B/H}(k), \quad k = 0, \ldots, N-1.$$

Then, Eqs. (2.7) and (2.8) imply

$$\begin{aligned} x(k) &= \textstyle\sum_l^{j-1} H_L(k-2l)\, \tilde{y}_L(l) + H_B(k-2l)\, \tilde{y}_B(l) + H_H(k-2l)\, \tilde{y}_H(l) \\ &= \textstyle\sum_l^{j-1} \langle \mathbf{x}, \tilde{\varphi}^1_L(\cdot - 2l) \rangle \, \varphi^1_L(k-2l) + \langle \mathbf{x}, \tilde{\varphi}^1_B(\cdot - 2l) \rangle \, \varphi^1_B(k-2l) + \langle \mathbf{x}, \tilde{\varphi}^1_L(\cdot - 2l) \rangle \, \varphi^1_H(k-2l). \end{aligned} \quad (2.12)$$

Thus, if the perfect reconstruction condition (2.11) is satisfied then the set of two-sample shifts of the signals $\tilde{\varphi}^1_{L/B/H}$ and $\varphi^1_{L/B/H}$ form a bi-frame for the signal space. If $\mathbf{P}(n) = c\tilde{\mathbf{P}}^T(n)$, $n = 0, \ldots, N-1$, then the signals $\varphi^1_{L/B/H}$ generate a tight frame.

2.2.1 Multiscale frame transform

In order to extend the frame transform to its coarse scale, we have to apply the analysis filter bank to the signal $\tilde{\mathbf{y}}_L^1 = \{\tilde{y}_L^1(k)\}$, which is the output from the low-pass filter $\widetilde{\mathbf{H}}_L$. However, the signal $\tilde{\mathbf{y}}_L^1$, unlike the signal $\mathbf{x}$ and the filter bank, is $N/2$-periodic. Therefore, the filter banks should be modified to become $N/2$-periodic. We re-denote the filter banks $\widetilde{\mathbf{F}} = \left\{\widetilde{\mathbf{H}}_L, \widetilde{\mathbf{H}}_B, \widetilde{\mathbf{H}}_H\right\}$ and $\mathbf{F} = \{\mathbf{H}_L, \mathbf{H}_B, \mathbf{H}_H\}$ as $\widetilde{\mathbf{F}}^{\mathbf{1}} = \left\{\widetilde{\mathbf{H}}_L^1, \widetilde{\mathbf{H}}_B^1, \widetilde{\mathbf{H}}_H^1\right\}$ and $\mathbf{F}^{\mathbf{1}} = \left\{\mathbf{H}_L^1, \mathbf{H}_B^1, \mathbf{H}_H^1\right\}$, respectively, and call them the first-scale filter banks. The $N/2$-periodic filters, which constitute the second-scale filter banks $\widetilde{\mathbf{F}}^{\mathbf{2}}$ and $\mathbf{F}^{\mathbf{2}}$, are defined via their DFTs:

$$\widehat{\widetilde{H}}_{L/B/H}^{2}(n) \triangleq \widehat{\widetilde{H}}_{L/B/H}^{1}(2n), \quad \widehat{H}_{L/B/H}^{2}(n) \triangleq \widehat{H}_{L/B/H}^{1}(2n), \quad n = 0, \dots, N/2-1. \tag{2.13}$$

Obviously, the perfect reconstruction condition (2.11) remains true for these filter banks. However, any other $N/2$-periodic PRFB can be used for the second-scale transform.

Assume that the signals $\tilde{\mathbf{y}}_{L/B/H}^1$ are the output from the analysis filter bank $\widetilde{\mathbf{F}}^{\mathbf{1}}$. Application of the analysis filter bank $\widetilde{\mathbf{F}}^{\mathbf{2}}$ to the signal $\tilde{\mathbf{y}}_L^1$ produces three $N/4$-periodic signals

$$\tilde{y}_{L/B/H}^2(k) = \sum_l^{j-1} \tilde{h}_{L/B/H}^2(l-2k)\tilde{y}_{L/B/H}^1(l) = \sum_l^{j-1} \tilde{H}_{L/B/H}^2(l-2k) \sum_m^{j} \tilde{H}_L^1(m-2l)x(m)$$

$$= \sum_m^{j} x(m)\, \tilde{\varphi}_{L/B/H}^2(m-4k) = \langle \mathbf{x},\, \tilde{\varphi}_{L/B/H}^2(\cdot - 4k)\rangle, \tag{2.14}$$

where

$$\tilde{\varphi}_{L/B/H}^2(k) \triangleq \sum_l^{j-1} \tilde{H}_{L/B/H}^2(l)\tilde{\varphi}_L^1(k-2l),\ k = 0, \dots, N/4-1, \tag{2.15}$$

are $N/4$-periodic signals, which we call the second-scale discrete-time analysis framelets.

The signal $\tilde{\mathbf{y}}_L^1$ is restored as

$$\tilde{y}_L^1(k) = \sum_l^{j-2} H_L^2(k-2l)\, \tilde{y}_L^2(l) + H_B^2(k-2l)\, \tilde{y}_B^2(l) + H_H^2(k-2l)\, \tilde{y}_H^2(l). \tag{2.16}$$

Then, the following expansion of the original signal $\mathbf{x}$ holds

$$x(k) = \sum_l^{j-1} \langle \mathbf{x}, \tilde{\varphi}_B^1(\cdot - 2l)\rangle\, \varphi_B^1(k-2l) + \langle \mathbf{x}, \tilde{\varphi}_L^1(\cdot - 2l)\rangle\, \varphi_H^1(k-2l) \tag{2.17}$$

$$+ \sum_l^{j-2} \langle \mathbf{x}, \tilde{\varphi}_L^2(\cdot - 4l)\rangle\, \varphi_L^2(k-4l) + \langle \mathbf{x}, \tilde{\varphi}_B^2(\cdot - 4l)\rangle\, \varphi_B^2(k-4l) + \langle \mathbf{x}, \tilde{\varphi}_L^2(\cdot - 4l)\rangle\, \varphi_H^2(k-4l),$$

where $\varphi_{L/B/H}^2(k) \triangleq \sum_l^{j-2} H_{L/B/H}^2(l)\varphi_L^1(l-2k)$.

By successive application of the filter bank to the output from the low-pass filter, we obtain the multiscale expansion of the signal $\mathbf{x}$:

$$x(k) = \sum_{r=1}^{m} \sum_{l}^{j-r} \langle \mathbf{x}, \tilde{\varphi}_B^r(\cdot - 2^r l) \rangle \, \varphi_B^r(k - 2^r l) + \langle \mathbf{x}, \tilde{\varphi}_L^r(\cdot - 2^r l) \rangle \, \varphi_H^r(k - 2^r l)$$
$$+ \sum_{l}^{j-m} \langle \mathbf{x}, \tilde{\varphi}_L^m(\cdot - 2^m l) \rangle \, \varphi_L^m(k - 2^m l), \quad m < j,$$

where

$$\tilde{\varphi}_{L/B/H}^r(k) \triangleq \sum_{l}^{j-r} \tilde{H}_{L/B/H}^r(l) \tilde{\varphi}_L^{r-1}(l - 2k), \quad \varphi_{L/B/H}^r(k) \triangleq \sum_{l}^{j-r} H_{L/B/H}(l) \varphi_L^{r-1}(l - 2k). \tag{2.18}$$

Thus, the discrete-time framelets $\{\tilde{\varphi}_B^r,\ \tilde{\varphi}_H^r,\ \tilde{\varphi}_L^m\}$ and $\{\varphi_B^r,\ \varphi_H^r,\ \varphi_L^m\}$, $r = 1, \ldots, m < j$, generate a bi-frame in the signal space $\mathfrak{S}^j$.

2.3 Interpolatory frames

In this section, we describe how to construct frames in the signal space starting from any pair of low-pass interpolatory filters or from a single filter. The problem reduces to the design of a perfect reconstruction filter bank with the desired properties. The key point in this design is the factorization scheme of a polyphase matrix.

A filter $\mathbf{H}$ is called interpolatory if its even polyphase component $\widehat{H}^e(n) = \text{const}$. We introduce an analysis–synthesis pair $\widetilde{\mathbf{H}}_L$ and $\mathbf{H_L}$ of low-pass interpolatory filters via their DFT:

$$\widehat{\widetilde{H}}_L(n) \triangleq \frac{\sqrt{2}}{2} \left(1 + \omega^{-n} \tilde{U}(2n)\right), \quad \widehat{H}_L(n) \triangleq \frac{\sqrt{2}}{2} \left(1 + \omega^{-n} U(2n)\right). \tag{2.19}$$

Assume that $\tilde{\mathbf{U}}$ and $\mathbf{U}$ are low-pass filters, $\tilde{U}(0) = U(0) = 1$. In addition, the symmetry relations

$$\omega^{-n} \tilde{U}(2n) = \omega^n \tilde{U}(-2n), \quad \omega^{-n} U(2n) = \omega^n U(-2n), \quad n = 0, \ldots, N/2 - 1, \tag{2.20}$$

hold. The polyphase matrices for the filter banks $\tilde{\mathbf{F}} \triangleq \left\{\widetilde{\mathbf{H}}_\mathbf{L}, \widetilde{\mathbf{H}}_\mathbf{B}, \widetilde{\mathbf{H}}_\mathbf{H}\right\}$ and $\mathbf{F} \triangleq \{\mathbf{H_L}, \mathbf{H_B}, \mathbf{H_H}\}$, which contain the above interpolatory low-pass filters, are

$$\tilde{\mathbf{P}}(n) = \begin{pmatrix} 1/\sqrt{2} & \tilde{U}(n)/\sqrt{2} \\ \widehat{\widetilde{H}}_B^e(n) & \widehat{\widetilde{H}}_B^o(n) \\ \widehat{\widetilde{H}}_H^e(n) & \widehat{\widetilde{H}}_H^o(n) \end{pmatrix}, \quad \mathbf{P}(n) \triangleq \begin{pmatrix} 1/\sqrt{2} & \widehat{H}_B^e(n) & \widehat{H}_H^e(n) \\ \widehat{U}(n)/\sqrt{2} & \widehat{H}_B^o(n) & \widehat{H}_H^o(n) \end{pmatrix}.$$

Then, the perfect reconstruction condition (2.11) leads to the equation:

$$\mathbf{R}(n) \cdot \widetilde{\mathbf{R}}(-n) = \frac{1}{2} \mathbf{Q}(n), \tag{2.21}$$

where

$$\widetilde{\mathbf{R}}(n) \triangleq \begin{pmatrix} \widetilde{\widehat{H}}_B^e(n) & \widetilde{\widehat{H}}_B^o(n) \\ \widetilde{\widehat{H}}_H^e(n) & \widetilde{\widehat{H}}_H^o(n) \end{pmatrix}, \quad \mathbf{R}(n) \triangleq \begin{pmatrix} \widehat{H}_B^e(n) & \widehat{H}_H^e(n) \\ \widehat{H}_B^o(n) & \widehat{H}_H^o(n) \end{pmatrix},$$

$$\mathbf{Q}(n) \triangleq \begin{pmatrix} 1 & -\tilde{U}(-n) \\ -U(n) & 2 - U(n)\tilde{U}(-n) \end{pmatrix}.$$

Therefore, the construction of a frame with the interpolatory low-pass filters $\widetilde{\mathbf{H}}_L$ and $\mathbf{H_L}$ reduces to factorization of the matrix $\mathbf{Q}(n)$ as in (2.21). There are many options for $\mathbf{Q}(n)$ factorization. We describe the implications of the simplest triangular factorization:

$$\widetilde{\mathbf{R}}(n) = \frac{1}{\sqrt{2}} \begin{pmatrix} 0 & \tilde{w}(n) \\ 1 & -\tilde{U}(n) \end{pmatrix}, \ \mathbf{R}(n) = \frac{1}{\sqrt{2}} \begin{pmatrix} 0 & 1 \\ w(n) & -U(n) \end{pmatrix}, \text{ where}$$

$$w(n)\tilde{w}(-n) = 2W(n), \quad W(n) \triangleq 1 - U(n)\tilde{U}(-n). \tag{2.22}$$

Thus, to complete the construction, we have to factorize the function $W(n)$. As soon as it is done, we obtain the perfect reconstruction filter bank, whose DFTs are

$$\begin{aligned} \widetilde{\widehat{H}}_L(n) &= \frac{\sqrt{2}}{2}\left(1 + \omega^{-n}\tilde{U}(2n)\right), & \widehat{H}_L(n) &= \frac{\sqrt{2}}{2}\left(1 + \omega^{-n}U(2n)\right), \\ \widetilde{\widehat{H}}_B(n) &= \frac{\omega^{-n}}{\sqrt{2}}\tilde{w}(2n), & \widehat{H}_B(n) &= \frac{\omega^{-n}}{\sqrt{2}}w(2n), \\ \widetilde{\widehat{H}}_H(n) &= \frac{\sqrt{2}}{2}\left(1 - \omega^{-n}\tilde{U}(2n)\right), & \widehat{H}_H(n) &= \frac{\sqrt{2}}{2}\left(1 - \omega^{-n}U(2n)\right). \end{aligned} \tag{2.23}$$

Note that in this case, the filters $\widetilde{\mathbf{H}}_\mathbf{H}$ and $\mathbf{H_H}$ are interpolatory. Since $U(0) = \tilde{U}(0) = 1$, these filters are high-pass. The filters $\widetilde{\mathbf{H}}_\mathbf{B}$ and $\mathbf{H_B}$ have no even polyphase component. Due to the symmetry property (2.20), the filters $\widetilde{\mathbf{H}}_\mathbf{L}$, $\mathbf{H_L}$, $\widetilde{\mathbf{H}}_\mathbf{H}$ and $\mathbf{H_H}$ are symmetric about zero in time domain. This filter bank generates a bi-frame in the signal space $\mathfrak{S}^j$.

2.4 Tight and semi-tight frames

If $U(n) = \tilde{U}(n)$ then we get $\widetilde{\mathbf{H}}_\mathbf{L} = \mathbf{H_L}$, $\widetilde{\mathbf{H}}_\mathbf{H} = \mathbf{H_H}$ and

$$W(n) = 2\left(1 - |U(n)|^2\right). \tag{2.24}$$

If the inequalities

$$|U(n)| \le 1, \quad n = 0, \dots, N-1, \tag{2.25}$$

hold then the function $W(n)$ can be factored as $W(n) = w(n)\, w(-n)$. Then, we have $\widetilde{\mathbf{H}}_\mathbf{B} = \mathbf{H_B}$.

If the condition (2.25) is not satisfied, we are still able to generate frames, which are very close to tight frames and, sometimes, may have advantages over tight frames. We get it if we take the same

high-pass and low-pass filters as were taken for the tight frame, while allowing the synthesis band-pass filter to be different from the analysis filter. Namely,

$$\begin{aligned}
&\widehat{\widetilde{H}}_L(n) = \widehat{H}_L(n) = \frac{\sqrt{2}}{2}\left(1+\omega^{-n}\,U(2n)\right),\\
&\widehat{\widetilde{H}}_B(n) = \frac{\omega^{-n}}{\sqrt{2}}\tilde{w}(2n), \quad \widehat{H}_B(n) = \frac{\omega^{-n}}{\sqrt{2}}w(2n), \quad w(n)\tilde{w}(-n) = W(n),\\
&\widehat{\widetilde{H}}_H(n) = \widehat{H}_H(n) = \frac{\sqrt{2}}{2}\left(1-\omega^{-n}U(2n)\right).
\end{aligned} \tag{2.26}$$

We refer to such a frame as a *semi-tight* frame. Due to the symmetry of $W(2n)$, a factorization of type (2.26), which provides (anti)symmetric band-pass filters, is always possible. Therefore, even when (2.25) holds, sometimes it is preferable to construct a semi-tight rather than a tight frame. On the other hand, in the semi-tight frames we can swap the approximation properties between the analysis and synthesis framelets.

2.5 Butterworth frames

Denote

$$U^{2r}(2n) \triangleq \omega^n \frac{\left(\cos\frac{\pi n}{N}\right)^{2r} - \left(\sin\frac{\pi n}{N}\right)^{2r}}{D(2n)}, \quad D(2n) \triangleq \left(\cos\frac{\pi n}{N}\right)^{2r} + \left(\sin\frac{\pi n}{N}\right)^{2r}. \tag{2.27}$$

It was explained in [1] how this function was derived from discrete splines. Obviously, $U^{2r}(0) = 1$, $|U^{2r}(2n)| \le 1$ for all n and $\omega^n U^{2r}(-2n) = \omega^{-n}U^{2r}(2n)$. Therefore, we can use this function for the construction of interpolatory frames as it was described in Section 2.4. Note that the denominator of $U^{2r}(2n)$ is strictly positive for any $n \in \mathbb{Z}$.

2.5.1 Tight and semi-tight frames

Let $\widetilde{U}(n) = U(n) = U^{2r}(n)$. Then, according to (2.26), the low- and high-pass filters are

$$\begin{aligned}
&\widehat{\widetilde{H}}_L(n) = \widehat{H}_L(n) = \frac{\sqrt{2}}{2}\left(1+\omega^{-n}\,U^{2r}(2n)\right) = \frac{\sqrt{2}\left(\cos\frac{\pi n}{N}\right)^{2r}}{D(2n)},\\
&\widehat{\widetilde{H}}_B(n) = \frac{\omega^{-n}}{\sqrt{2}}\tilde{w}(2n), \quad \widehat{H}_B(n) = \frac{\omega^{-n}}{\sqrt{2}}w(2n), \quad w(n)\tilde{w}(-n) = W(n),\\
&\widehat{\widetilde{H}}_H(n) = \widehat{H}_H(n) = \frac{\sqrt{2}}{2}\left(1-\omega^{-n}\,U^{2r}(2n)\right) = \frac{\sqrt{2}\left(\sin\frac{\pi n}{N}\right)^{2r}}{D(2n)}.
\end{aligned} \tag{2.28}$$

We need to factorize the function

$$W(2n) = 2\left(1-|U(2n)|^2\right) = \frac{2\left(\sin\frac{2\pi n}{N}\right)^{2r}}{2^{2r-2}D^2(2n)} = \frac{2(-1)^r\left(\omega^n-\omega^{-n}\right)^{2r}}{2^{4r-2}D^2(2n)}. \tag{2.29}$$

Tight frames: To get a tight frame, we need to factorize $W(2n)$ such that for all n $w(2n) = \tilde{w}(2n)$. It becomes true for

$$w(2n) = \tilde{w}(2n) = \frac{\sqrt{2}}{D(2n)} \times \begin{cases} 2^{1-r} \left(\sin \frac{2\pi n}{N}\right)^r, & \text{if } r \text{ is even;} \\ 2^{1-2r} \left(\omega^{2n} - 1\right)^r & \text{if } r \text{ is odd.} \end{cases} \tag{2.30}$$

If r is even then the band-pass filter $\mathbf{H}_B$ is symmetric, otherwise it is anti-symmetric. Both the low- and high-pass filters are symmetric in time domain.

Semi-tight frames: In this case, the low- and high-pass filters remain the same as in the tight frame case. However, we have more freedom in the factorization of $W(2n)$. In particular, the symmetric factorization is possible with any r:

$$\tilde{w}(2n) = \frac{\sqrt{2}\left(\sin \frac{2\pi n}{N}\right)^{2p}}{2^{p-1} D(2n)}, \quad w(2n) = \frac{\sqrt{2}\left(\sin \frac{2\pi n}{N}\right)^{2(r-p)}}{2^{2r-p-1} D(2n)}. \tag{2.31}$$

Note that all the designed filters are rational function of ω^n with non-vanishing denominators. The filters $\mathbf{H_L}$ are the low-pass half-band Butterworth filters, whereas $\mathbf{H_H}$ are the high-pass Butterworth filters (see [10, 1]). Therefore, we call the derived frames the Butterworth frames.

2.5.2 Quasi-vanishing moments (QVM)

One property of wavelets, which is important for applications, is the vanishing moments property, which annihilates polynomials of certain degrees that are convolved with the wavelet. Since we stay in the periodic setting, the convolution with polynomials is not possible. Therefore, we introduce the notion of quasi-vanishing moments (QVM). We call an $N-$periodic sequence $\mathbf{q_m} \stackrel{\Delta}{=} \{\mathbf{q_m(k)}\}_{\mathbf{k}\in\mathbb{Z}}$ the discrete quasi-polynomial of degree m if for $k = 0, \ldots, N-1$, $q_m(k) = P_m(k/N)$, where P_m is a polynomial of degree m.

Definition 2.2 *We say that a discrete-time framelet $\varphi \in \mathfrak{S}^{\mathfrak{j}}$ has $m+1$ QVM if there exists a natural number $s < N/2$ such that for any discrete quasi-polynomial $\mathbf{q_m}$ of degree m $r(k) \stackrel{\Delta}{=} \sum_l^j \varphi(k-l) q_m(l) = 0$ for $k = s, \ldots, N-s$.*

Proposition 2.1 *Assume that the DFT of a high-pass filter $\widehat{H}_H(n) \in \mathfrak{S}^{\mathfrak{j}}$ is a rational function of ω^n with non-vanishing denominator, which comprises the factor $(1-\omega^n)^m$ (or $\sin^m(\pi n/N)$) in its numerator. Then, provided $m < 2^{j-1} - 2$, the corresponding discrete-time framelet of the first scale $\varphi_H^1 \in \mathfrak{S}^{\mathfrak{j}-\mathfrak{1}}$ has $m+1$ QVM. This remains true for the coarser scales framelets $\varphi_H^t \in \mathfrak{S}^{\mathfrak{j}-\mathfrak{t}}$, provided $m < 2^{j-1-t} - 2$. A similar statement holds for the band-pass filter $\widehat{H}_B(n) \in \mathfrak{S}^{\mathfrak{j}}$.*

Equations (2.28) and (2.30) imply that, if framelets are designed using the function $U^{2r}(n)$, then the framelets φ_H^t have $2r$ QVM. In the case of a tight frame, the framelets φ_B^t have r QVM. In the

semi-tight frame, it stems from Eq. (2.31) that we can swap QVM between the analysis framelets $\widetilde{\varphi}_B^t$ ($2p$ QVM) and the synthesis framelets φ_B^t ($2r - 2p$ QVM). Practically, it is advisable to have more QVM in the analysis framelets.

2.6 Examples

We display the frequency responses (FR) of a few filter banks, which produce tight and semi-tight Butterworth frames. We assign a filter bank the order r if it originates from the function U^{2r}, as it is described in Section 2.4. In this case, the high-pass filter has $2r$ QVM. The band-pass filter, which produces the tight frame, has r QVM. The band-pass filters for the semi-tight frames have $2(r - p)$ QVM.

In Fig. 1 we illustrate tight frames of the first and tenth order. The two left pictures display the FR of the filters of first order and the corresponding framelets of the sixth scale. The high-frequency and low-frequency framelets are symmetric, while mid-frequency framelet is anti-symmetric. The high-pass filter has two QVM, while the band-pass filter has only one QVM. The two right pictures display the FR of the filters of the tenth order and the corresponding framelets of the sixth scale. All the framelets are symmetric. The high-pass filter has twenty QVM, while the band-pass filter has ten QVM. We emphasize that the FR of low- and high-pass filters are the mirrored versions of each other and their shape is close to rectangular.

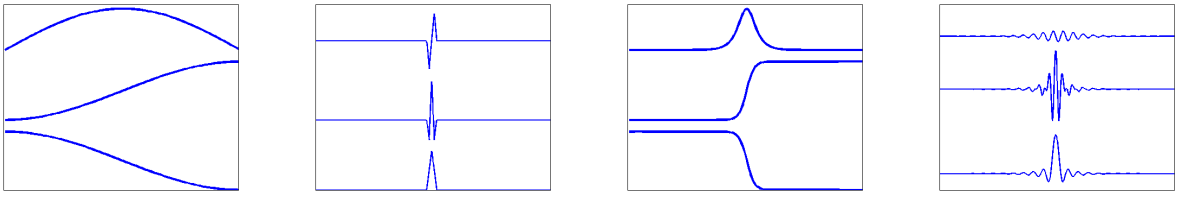

Figure 1: Left to right: 1. The FR of tight frame filters of the first order. 2. The corresponding framelets of the sixth scale. 3. The FR of the tight frame filters of the tenth order. 4. The corresponding framelets of the sixth scale.

Figure 2 illustrates tight and semi-tight frames of the third order. The two left pictures display the FR of the filters and the corresponding framelets of the sixth scale for the tight frame. The high-frequency and low-frequency framelets are symmetric, while the mid-frequency framelet is anti-symmetric. The high-pass filter has six QVM, while the band-pass filter has three QVM. The shape of the low- and high-pass filters approaches a rectangular shape but not as far as the shape of the tenth-order filters. The two right pictures present the FR of different band-pass filters of the third order and the corresponding framelets of the sixth scale. The bottom pictures display the analysis filter for the semi-tight frame, which has four QVM and the corresponding framelet, which is symmetric. The

top pictures display the synthesis filter for the same semi-tight frame, which has two QVM and the corresponding framelet, which is symmetric. The middle pictures display the synthesis filter for the tight frame, which has three QVM and the corresponding framelet, which is anti-symmetric.

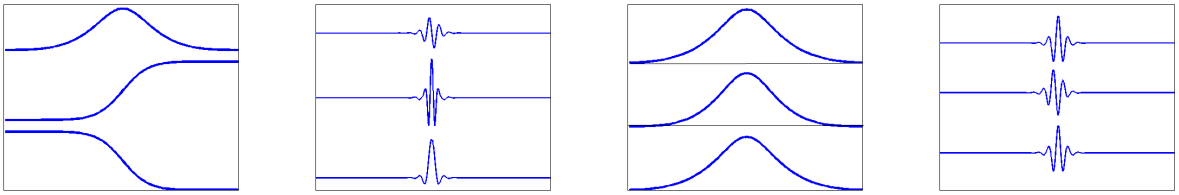

Figure 2: Left to right: 1. The FR of tight frame filters of the third order. 2. The corresponding framelets of the sixth scale. 3. The FR of the band-pass filters of third order: top – semi-tight with two QVM, middle – tight with three QVM, bottom – semi-tight with four QVM. 4. The corresponding framelets of the sixth scale.

3 Regularization of Butterworth frames

3.1 Why wavelet frames are good for denoising

We display in Fig. 3 the spectra of the discrete-time framelets φ_H^r, φ_B^r, $r = 1, 2, 3, 4$ and φ_L^4, which implement the four-scale tight frame transform of the third order.

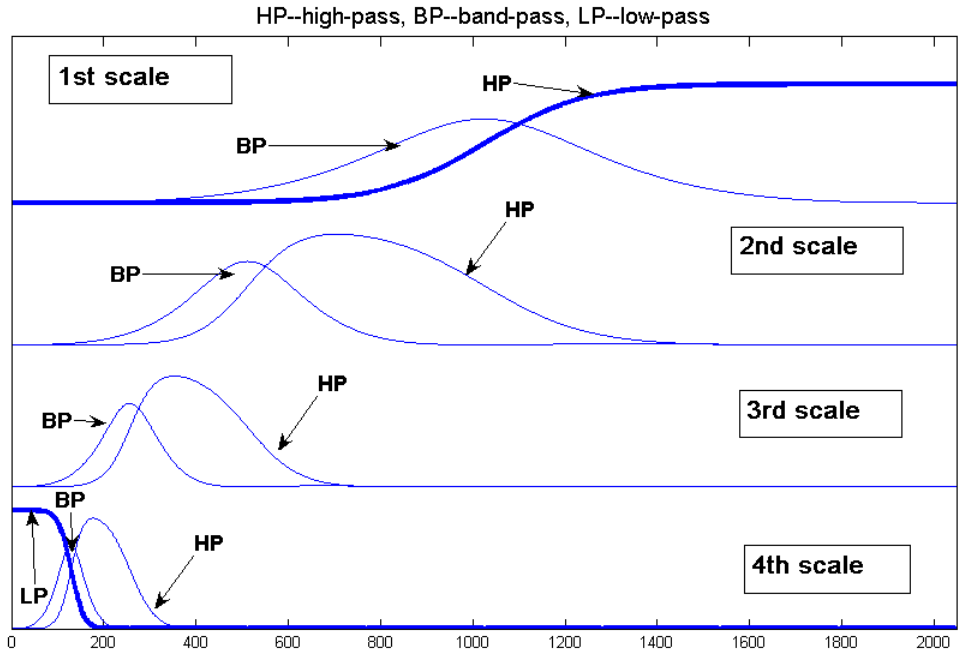

Figure 3: Spectra of the discrete-time framelets φ_H^r, φ_B^r, $r = 1, 2, 3, 4$ and φ_L^4. LP (low-pass) is related to φ_L^4, HP (high-pass) is related to φ_H^r, BP (band-pass) is related to φ_B^r.

We can see that the spectra, which are displayed in Fig. 3, form at least two-fold coverage of the frequency domain of the signal except for the frequency bands, which are covered by the spectra of the low-frequency framelet φ_L^4 and the high-frequency framelet φ_H^1. They are boldfaced in Fig. 3. When the signal is corrupted by a Gaussian noise, its energy is dispersed among bigger number of coefficients compared to the wavelet transforms and, therefore, typically, the signal-to-noise ratio (SNR) in the transform domain is higher than that in the wavelet transform domain. It is not true for the coefficients related to the framelets φ_L^4 and φ_H^1. But the SNR in the sparse low-frequency block of coefficients related to φ_L^4 is much higher than in the original signal. Therefore, no denoising procedures are applied to this block. On the other hand, the block of high-pass coefficients related to φ_H^1 is the most populated ($N/2$ coefficients). But, due to the vanishing moments property of the framelets, this block contains relatively small number of significant coefficients, which correspond to sharp transients in the signal (sharp edges in the image). All the rest of the coefficients are noise-born. Therefore, the content of this block should be significantly suppressed if not discarded completely.

Figure 4 displays the coefficients of the four-scale framelet transform of one column in the "Barbara" image (Figure 7) (except for the low-frequency block related to φ_L^4). The left picture displays the framelet transform of a clean signal. The central picture displays the transform of the moderately noised signal (STD=10). The transform of the strongly noised signal (STD=100) is shown in the right

picture. The grid separates blocks of coefficients in the following way:

Interval	(0,H4)	(H4,B4)	(B4,H3)	(H3,B3)	(B3,H2)	(H2,B2)	(B2,H1)	(H1,B1)
Coeff. of framelet	φ_H^4	φ_B^4	φ_H^3	φ_B^3	φ_H^2	φ_B^2	φ_H^1	φ_B^1

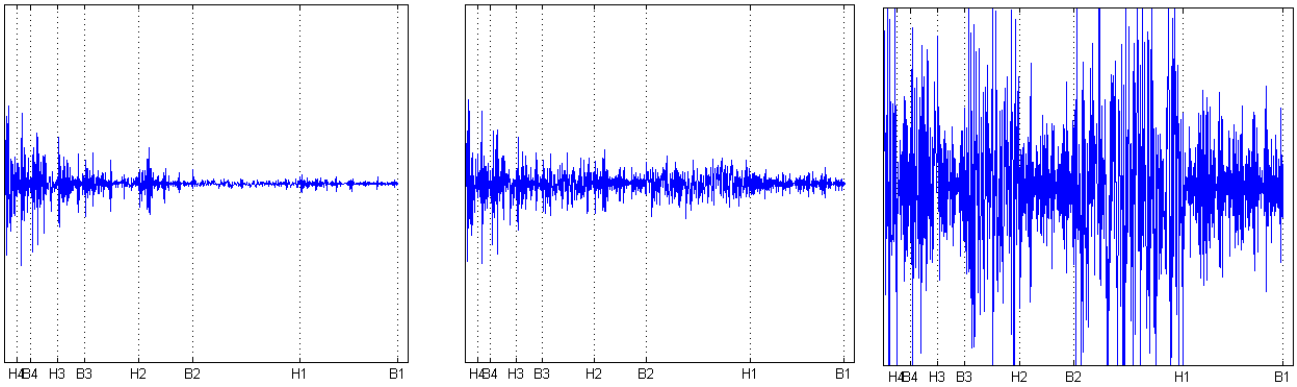

Figure 4: Left: four-scale of the framelet transform in a clean signal. Center: transform of the moderately noised signal (STD=10). Right: transform of the strongly noised signal (STD=100).

When the noise is moderate, the coherent structure of the signal is clearly seen in blocks of coefficients except for the block related to φ_H^1. In this case, adaptive thresholding schemes proved to be efficient. However, when the noise is strong, thresholding results either in oversmoothing the signal or in generating multiple artifacts. We propose a new method of frame-based image denoising, which retrieves the coherent structure of the image from strongly noised original, without generating artifacts.

3.2 Regularized Butterworth frames

The DFT of the high- and low-pass filters defined above comprise the factors $\sin^{2r}\frac{\pi n}{N}$. Therefore, application of these filters to a signal reduces to the $2r$-th numerical order differentiation. Typically, this operation enhances the noise level. We propose to modify these filters using a method based on Tikhonov regularization [15]. Thus, we achieve significant suppression of the noise while retaining the coherent structure of the signal without producing artifacts.

3.2.1 Design of regularized filters

Assume that the DFT $\widehat{H}(n)$ of a filter $\mathbf{H}$ comprises the factor $\sin^{2r}\frac{\pi n}{N}$ for some $r \in \mathbb{N}$. Then, it can be regarded as the circular convolution operator, which is the inversion of a circular convolution operator $\mathbf{G}$. The operator $\mathbf{G}$ is the filter and its DFT is $\widehat{G}(n) = 1/\widehat{H}(n)$. Therefore, the operator $\mathbf{G}$ is defined

on the subspace of signals, $\mathbf{x}$, whose DFT can be represented as

$$\widehat{x}(n) = \Big(\frac{\pi n}{N}\Big)^{2r} \cdot b(n), \quad \frac{1}{b(n)} \neq 0,\ n = 0, \dots N-1. \tag{3.32}$$

Thus, the signal $\mathbf{x}$, which is the output from the application of the filter $\mathbf{H}$ to the signal $\mathbf{y}$, is the solution of the convolution equation

$$\mathbf{y} = \mathbf{G} \star \mathbf{x}, \tag{3.33}$$

where $\star$ denotes the circular convolution.

Since the signal $\mathbf{y}$ is strongly corrupted by noise, the exact solution becomes highly irregular. Therefore, it is reasonable not to pursue the exact solution of Eq. (3.33) but to obtain $\mathbf{x}$ as

$$\mathbf{x} = \operatorname{argmin}_{\mathbf{f}} J_\rho(\mathbf{f}), \quad J_\rho(\mathbf{f}) \stackrel{\Delta}{=} \rho I(\mathbf{f}) + D(\mathbf{f}, \mathbf{y}), \tag{3.34}$$

where $\mathbf{f}$ are N-periodic signals, which satisfy the condition (3.32). The penalty functional

$$I(\mathbf{f}) \stackrel{\Delta}{=} \|\mathbf{f}\|^2 + \|\Delta \mathbf{f}\|^2 = \sum_k^j f^2(k) + \sum_k^j (f(k+1) - f(k))^2 = \frac{1}{N} \sum_n^j |\widehat{f}(n)|^2 \left(1 + 4 \sin^2 \frac{\pi n}{N}\right) \tag{3.35}$$

allows to control the regularity of the solutions, whereas the discrepancy functional

$$D(\mathbf{f}) \stackrel{\Delta}{=} \|\mathbf{G} \star \mathbf{f} - \mathbf{y}\|^2 = \sum_n^j |\widehat{f}(n)\, \widehat{G}(n) - \widehat{y}(n)|^2 = \frac{1}{N} \sum_n^j \left| \frac{\widehat{f}(n)}{\widehat{H}(n)} - \widehat{y}(n) \right|^2 \tag{3.36}$$

controls the approximation of the original signal $\mathbf{y}$ by the signal $\mathbf{G} \star \mathbf{f}$. The parameter ρ governs the trade-off between the regularity of the solution and the approximation of the original signal.

Denote $R(n) \stackrel{\Delta}{=} \left(1 + 4 \sin^2 \frac{\pi n}{N}\right)$. Equations (3.35) and (3.36) imply

$$N J_\rho(\mathbf{f}) = \sum_n^j |\widehat{f}(n)|^2 A_\rho(n) + 2\mathfrak{Re}\left(\widehat{f}(n) \widehat{G}(n) \overline{\widehat{y}(n)}\right) + |\widehat{y}(n)|^2,$$

where

$$A_\rho(n) \stackrel{\Delta}{=} \rho R(n) + |\widehat{G}(n)|^2 = |\widehat{G}(n)|^2 \left(\rho R(n) |\widehat{H}(n)|^2 + 1\right). \tag{3.37}$$

The functional $J_\rho(\mathbf{f})$ achieves its minimum when

$$\widehat{f}(n) = \frac{\overline{\widehat{G}(n)} \widehat{y}(n)}{A_\rho(n)} = \frac{\overline{\widehat{H}}(n) \widehat{y}(n)}{\rho R(n) |\widehat{H}(n)|^2 + 1} \tag{3.38}$$

and the solution becomes

$$\mathbf{x}_\rho = \mathbf{H}_\rho \star \mathbf{y}, \quad \widehat{H}_\rho(n) = \frac{\overline{\widehat{H}}(n)}{\rho R(n) |\widehat{H}(n)|^2 + 1}, \quad R(n) = 1 + 4 \sin^2 \frac{\pi n}{N}. \tag{3.39}$$

Obviously, condition (3.32) is satisfied.

Thus, filtering the signal $\mathbf{y}$ with the filter $\mathbf{H}$ is replaced by filtering with the modified filter $\mathbf{H}_\rho$. The filter $\mathbf{H}_\rho$ produces the same number of QVMs as the filter $\mathbf{H}$ but, unlike the latter, it suppresses the

higher frequencies, thus, adding regularity to the filtered signal. Increase of the parameter ρ enhances the suppression. Note that $\mathbf{H}_0 = \mathbf{H}$.

If we have an estimated σ of the standard deviation of the noise in the signal $\mathbf{y}$ to be filtered, then, we can evaluate a quasi-optimal value of the parameter ρ from the equation

$$\delta(\rho) \stackrel{\Delta}{=} D(\mathbf{x}_\rho) = (N-1)\sigma^2. \tag{3.40}$$

Proposition 3.1 *Equation (3.40) has a unique solution .*

Proof: Equations (3.36) and (3.39) imply

$$\delta(\rho) = \frac{1}{N}\sum_{n}^{j} |\widehat{y}(n)|^2 \left(\frac{1}{\rho R(n)|\widehat{H}(n)|^2 + 1} - 1\right)^2.$$

Obviously, $\delta(0) = 0$ and $\delta(\rho)$ grows monotonically approaching the value $\delta(\infty) = \|y\|^2 \geq (N-1)\sigma^2$. ■

The function $\delta(\rho)$ can be explicitly calculated.

Remark Assume that the set of filters $\left\{\widetilde{\mathbf{H}}_\mathbf{L}, \widetilde{\mathbf{H}}_\mathbf{B}, \widetilde{\mathbf{H}}_\mathbf{H}\right\}$ and $\{\mathbf{H_L}, \mathbf{H_B}, \mathbf{H_H}\}$ form a perfect reconstruction filter bank. If the high- and band-pass analysis filters are modified according to the above scheme then the modified analysis filter bank $\widetilde{\mathbf{F}}_\rho \stackrel{\Delta}{=} \left\{\widetilde{\mathbf{H}}_\mathbf{L}, \widetilde{\mathbf{H}}_{\mathbf{B},\rho}, \widetilde{\mathbf{H}}_{\mathbf{H},\rho}\right\}$ still generates a frame for the signal space $\mathfrak{S}^j$. There exist signal filter banks $\check{\mathbf{F}}_\rho$ such that the pairs $\widetilde{\mathbf{F}}_\rho$ and $\check{\mathbf{F}}_\rho$ form perfect reconstruction filter banks. But, in our method, we abandon the perfect reconstruction property and use for the reconstruction the regularized filter bank $\mathbf{F}_\rho \stackrel{\Delta}{=} \{\mathbf{H_L}, \mathbf{H}_{\mathbf{B},\rho}, \mathbf{H}_{\mathbf{H},\rho}\}$.

3.2.2 Examples

We display in Fig. 5 the FR of tight frame filters of the third order,which are regularized according to Eq. (3.39), for different parameters ρ. The left plot depicts the non-distorted filters when $\rho = 0$. The central plot depicts the filters when a moderate $\rho = 0.2$ was applied. We see that the high-frequency regions of the FR of the high- and band-pass filters are dumped. The case for $\rho = 3$ is illustrated in the right plot. Here, the FR of the band-pass and, especially, the high-pass filters are significantly shrunk.

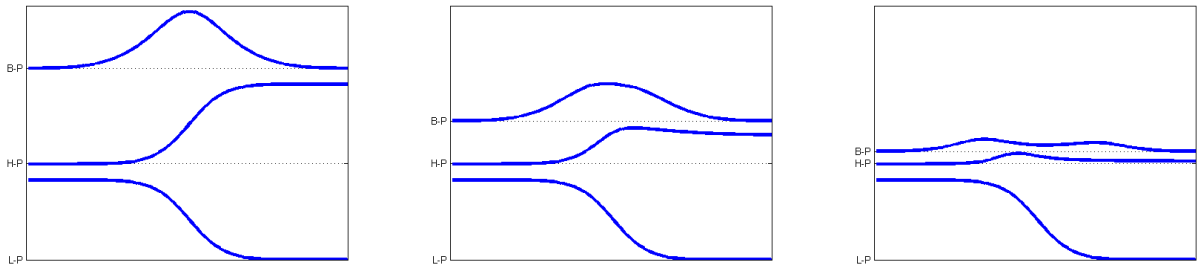

Figure 5: Left to right: 1. The FR of tight frame filters of the third order. 2. The FR of the modified filters as in (3.39) when $\rho = 0.2$. 3. The FR of the modified filters when $\rho = 3$.

We display in Fig. 6 the coefficients of the four-scale framelet transforms of one column from the "Barbara" image presented in Fig. 7 (except for the low-frequency block related to φ_L^4). Left picture displays the framelet transform of a clean signal, which is implemented by a tight frame filter bank of the third order. The central picture displays the same transform for a strongly noised signal (STD=100). The regularized transform of the noised signal is shown in the right picture. The regularized transform significantly reduces the noise level, while revealing some structural events.

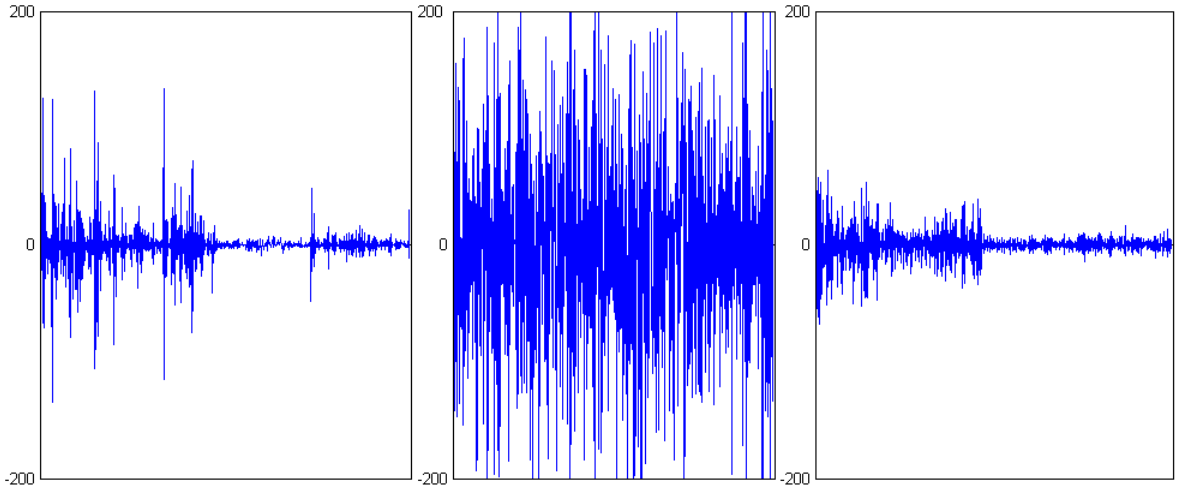

Figure 6: Left: Application of a four-scale tight frame transform to the clean signal. Center: Application of the same transform to a strongly noised signal (STD=100). Right: Application of the regularized transform to a noised signal.

4 Image denoising

Assume, we have an analysis $\widetilde{\mathbf{F}} \triangleq \left\{\widetilde{\mathbf{H}}_{\mathbf{L}}, \widetilde{\mathbf{H}}_{\mathbf{B}}, \widetilde{\mathbf{H}}_{\mathbf{H}}\right\}$ and a synthesis $\mathbf{F} \triangleq \{\mathbf{H_L}, \mathbf{H_B}, \mathbf{H_H}\}$ filter banks. Note that the pair of the filter banks $\widetilde{\mathbf{F}}$ and $\mathbf{F}$ do not necessarily form a perfect reconstruction filter bank. The application of a one-scale 2D framelet transform to an image $\mathbf{I}$ of size $N \times N$ is implemented in two steps:

1. The analysis filter bank $\widetilde{\mathbf{F}}$ is applied to the columns of the image $\mathbf{I}$ producing the coefficient matrix $\mathbf{C_{column}}$ consisting of three blocks $\mathbf{C_L}$, $\mathbf{C_B}$, $\mathbf{C_H}$ of size $N/2 \times N$ each.

2. The filter bank $\widetilde{\mathbf{F}}$ is applied to the rows of the sub-matrices $\mathbf{C_L}$, $\mathbf{C_B}$, $\mathbf{C_H}$ to produce the nine-block coefficient matrix $\mathbf{C}$ of size $3N/2 \times 3N/2$:

$$\mathbf{C}= \begin{array}{|c|c|c|} \hline \mathbf{C_{LL}} & \mathbf{C_{LB}} & \mathbf{C_{LH}} \\ \hline \mathbf{C_{BL}} & \mathbf{C_{BB}} & \mathbf{C_{BH}} \\ \hline \mathbf{C_{HL}} & \mathbf{C_{HB}} & \mathbf{C_{HH}} \\ \hline \end{array}$$

The reconstruction of the image is implemented in the reverse order:

1. The synthesis filter bank $\mathbf{F}$ is applied to the rows of the matrix $\mathbf{C}$ producing the coefficient matrix $\check{\mathbf{C}}_{\mathbf{column}}$ that consists of three blocks $\check{\mathbf{C}}_{\mathbf{L}}$, $\check{\mathbf{C}}_{\mathbf{B}}$, $\check{\mathbf{C}}_{\mathbf{H}}$ of size $N/2 \times N$ each.

2. The filter bank $\mathbf{F}$ is applied to the columns of $\check{\mathbf{C}}_{\mathbf{column}}$ producing the image $\check{\mathbf{I}}$.

The transform can be extended to coarser scales by the application of the same or another analysis filter bank to the block $\mathbf{C_{LL}}$ of the coefficient matrix $\mathbf{C}$.

4.1 Application of regularized filters

Framelet transforms with regularized Butterworth filter banks are proved to be efficient when the noise level is high. These filter banks suppress the noise, while revealing and preserving the coherent structure of the image.

We apply the multiscale transforms up to the fifth or sixth decomposition scale using framelets with different number of QVMs, which are derived by regularizing tight and semi-tight frames. An important feature of this algorithm is that the filter banks are different for different scales. On the one hand, the periodic filters are updated in an obvious way when applied to arrays of different size. But, on the other hand, we use different values for the parameter ρ for different filters and different scales. The reason for this is the following. As it is seen in Fig. 3, application of the high-pass filter to subsequent scales splits the frequency domain of a signal in a logarithmic way. The frequency of the band-pass filter for some scale occupies a frequency band, which is close to the frequency band

of the high-pass filter related to a previous scale. Typically, the coherent structure of a noised signal is contained in the lower region of the frequency domain. The signal-to-noise ratio (SNR) is different for the different blocks of the frame transform coefficients. As the coefficient block in the lower the frequency band is related to, the higher the SNR this block has. Therefore, the denoising strategy for different blocks should vary along with the frequency content of the block. This consideration is utilized in schemes, which apply different thresholds to different blocks of the wavelet transform coefficients [5, 6]. We do not threshold the coefficients. Instead, we change the parameter ρ.

Assume, the value of the parameter is $\rho = \rho_0$. The block of coefficients of the first decomposition scale resulting from the application of the high-frequency filter $\widetilde{\mathbf{H}}^{\mathbf{1}}_{\mathbf{H}}$ to a noisy signal consists almost completely from the noise component. Therefore, it requires a maximal suppression. We replace the filter $\widetilde{\mathbf{H}}^{\mathbf{1}}_{\mathbf{H}}$ by $\widetilde{\mathbf{H}}^{\mathbf{1}}_{\mathbf{H},\mathbf{4}\rho}$. The coefficients, produced by the first scale band-pass filter $\widetilde{\mathbf{H}}^{\mathbf{1}}_{\mathbf{B}}$, are related to the lower frequency band. Therefore, we modify the filter to be $\widetilde{\mathbf{H}}^{\mathbf{1}}_{\mathbf{B},\rho}$. The filters $\widetilde{\mathbf{H}}^{\mathbf{k}}_{\mathbf{H}}$ and $\widetilde{\mathbf{H}}^{\mathbf{k}}_{\mathbf{B}}$ operating on the subsequent scales $k = 2, ..., 5(6)$, are replaced by the regularized filters $\widetilde{\mathbf{H}}^{\mathbf{j}}_{\mathbf{H},\rho/\mathbf{2^{k-2}}}$ and $\widetilde{\mathbf{H}}^{\mathbf{j}}_{\mathbf{B},\rho/\mathbf{2^{k-1}}}$, respectively. The synthesis filters are modified similarly.

The denoising procedure of an image consists of the decomposition of the image into five or six scales using the regularized analysis filters. This is followed by the reconstruction that uses the regularized synthesis filters.

Note that we have at our disposal tight and semi-tight Butterworth framelets of any order. This enables to achieve better adaptation to the properties of the image under processing.

4.1.1 Experimental results

We applied the above algorithm to a number of benchmark images that were corrupted by strong Gaussian noise. We evaluate the quality of restored images by peak signal-to-noise ratio (PSNR)

$$PSNR \triangleq 10 \log_{10} \left(\frac{N\, 255^2}{\sum_{k,l=1}^{N} (x(k,l) - \tilde{x}(k,l))^2} \right) \, dB, \tag{4.41}$$

where $\{x(k,l)\}$ and $\{\tilde{x}(k,l)\}$ are the pixels of the clean and of the denoised images, respectively and by their visual appearance.

Barbara: We display in Fig. 7 the clean "Barbara" image and the image corrupted by Gaussian noise with STD=100, PSNR=8.13.

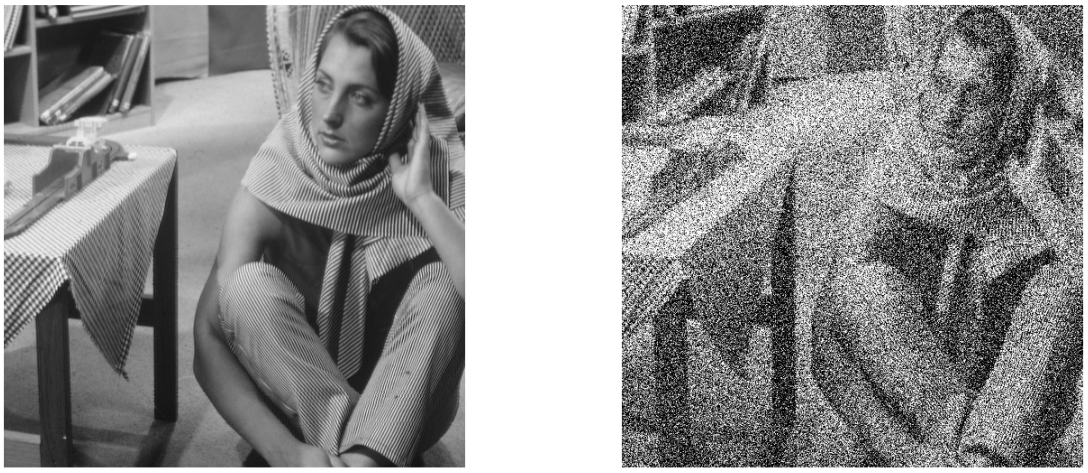

Figure 7: Left: Clean "Barbara" image. Right: The image corrupted by Gaussian noise with STD=100, PSNR=8.13.

We applied to the noised image the regularized framelets (RF) algorithm, where the framelets were derived from semi-tight frames of fifth order. The image was decomposed into five scales where $\rho = 0.97$. Then, it was subjected to repeated regularized processing with $\rho = 0.05$.

Figure **??** displays column # 50 from the noised image (thin line) versus the column from the clean image (thick line). Figure **??** does the same for the restored image. From Figs. **??**–**??** we see that the noise is significantly suppressed, while the shape of the curve is revealed and preserved.

In Fig. 8 we display the restored "Barbara" image. For comparison, we show the restored image after the application of the GSM algorithm ([7]). We see that the "GSM image" is cleaner than the "RF image" and its PSNR is higher. But it contains visual artifacts. Some edges are smeared. These drawbacks are not imminent to the "RF image".


Figure 8: Left: "Barbara" restored by the RF method, PSNR=21.02. Right: The image restored by the GSM method, PSNR=22.61.

We display in Fig. 9 the "Barbara" image that was corrupted by Gaussian noise with STD=200, with PSNR=2.11. The structure is almost completely buried by the noise. In the right picture, the image is restored by the application of the regularized framelets derived from semi-tight frames of the fifth order. The image was decomposed into five scales where $\rho = 2.06$.

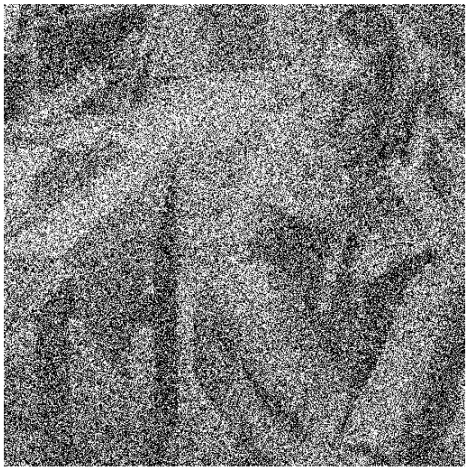


Figure 9: Left: Barbara corrupted by Gaussian noise with STD=200, PSNR=2.11. Right: The restored image, PSNR=19.56.

Boats: We display in Fig. 10 the clean "Boats" image and the image corrupted by Gaussian noise with STD=100, while PSNR=8.13.

Figure 10: Left: The clean "Boats" image. Right: The image corrupted by Gaussian noise with STD=100, PSNR=8.13.

We display in Fig. 11 the "Boats" image , which is restored by the application of the regularized framelets derived from semi-tight frames of the third order. The image was decomposed into five scales where $\rho = 2$. In the right picture we show the restored image after the application of GSM algorithm ([7]). This last image has many visual artifacts. The foreground texture is oversmoothed.

Figure 11: Left: "Boats" restored by the RF method, PSNR=21.67. Right: The image restored by the GSM method, PSNR=23.75.

We display in Fig. 12 the Boat image corrupted by a Gaussian noise with STD=200, while

PSNR=2.11. The image is buried almost completely in the noise. In the right picture, the image is restored by the application of regularized framelets derived from the semi-tight frames of the third order. The image was decomposed into five scales where $\rho = 2.5$. Then, it was subjected to repeated regularized processing with the parameter $\rho = 0.14$.

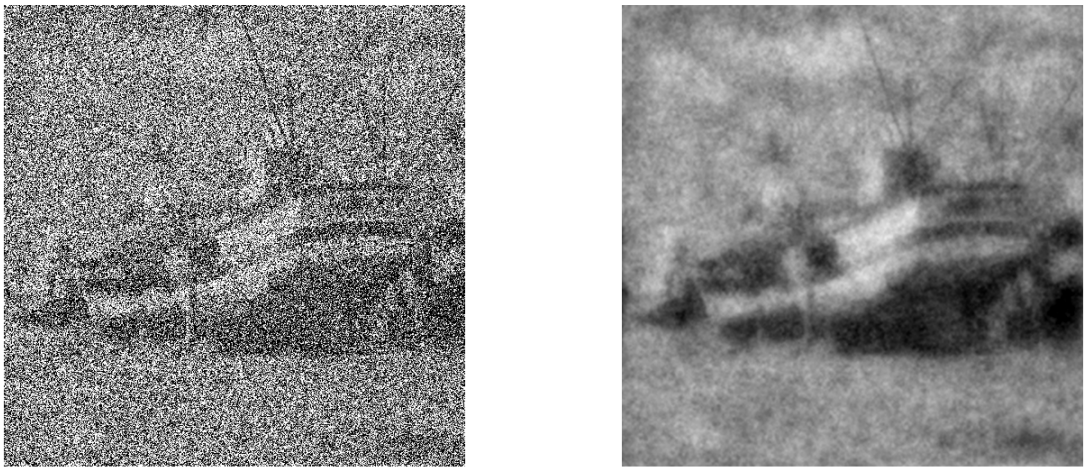

Figure 12: Left: Boat corrupted by a Gaussian noise with STD=200, PSNR=2.11. Right: The restored image, PSNR=20.46.

Lena: We display in Fig. 13 the clean "Lena" image and the image that was corrupted by a Gaussian noise with STD=100, PSNR=8.13.

Figure 13: Left: Clean "Lena" image. Right: The image corrupted by Gaussian noise with STD=100, PSNR=8.13.

Figure 14 displays the "Lena" image, which is restored by the application of the regularized framelets that wwere derived from the semi-tight frames of the fifth order. The image was decomposed into five scales where $\rho = 1.07$. In the right picture we show the restored image after the application of the GSM algorithm. The GSM based image is smoother than the RH based image and achieves much higher PSNR while some edges are eliminated and others are distorted.

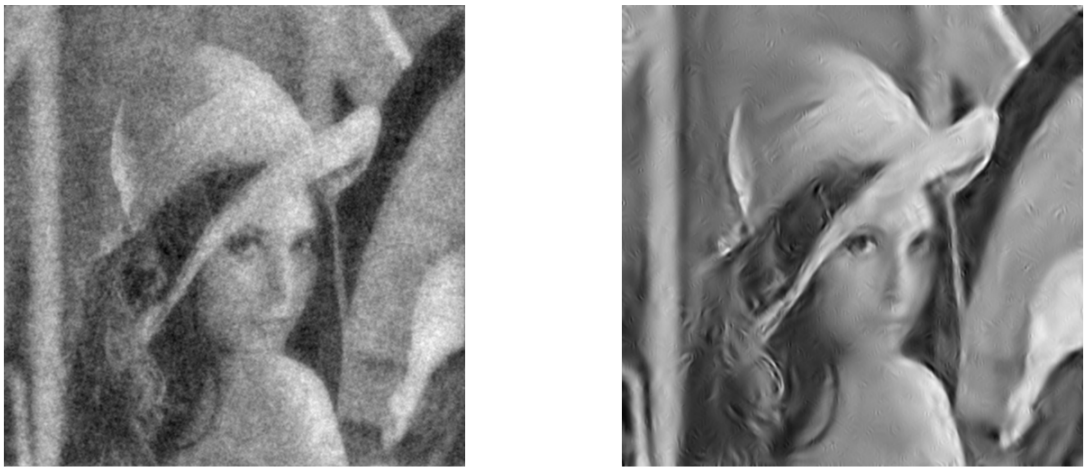

Figure 14: Left: The restored"Lena" image by the RF algorithm, PSNR=23.08. Right: The image is restored by the GSM algorithm, PSNR=25.64.

We display in Fig. 15 the "Lena" image corrupted by a Gaussian noise with STD=200, while PSNR=2.11. The structure is buried almost completely in the noise. In the right picture, the image is restored by the application of the regularized framelets that were derived from the semi-tight frames of the fifth order. The image was decomposed into five scales where $\rho = 2.25$. Then, it was subjected to repeated regularized processing with $\rho = 0.05$.

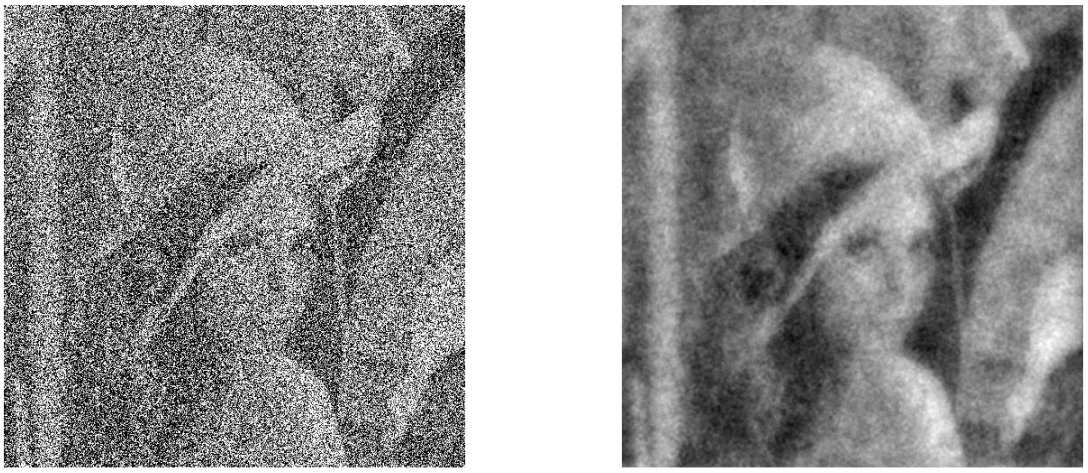

Figure 15: Left: "Lena" corrupted by a Gaussian noise with STD=200, PSNR=2.11. Right: The restored image, PSNR=21.13.

Figure 16: Clean images. Left: Goldhill. Right: Fingerprint.

Goldhill: We display in Fig. 17 the Goldhill image corrupted by a Gaussian noise with STD=100, while PSNR=8.13. In the right picture, the image, which was restored by the application of the regularized framelets derived from semi-tight frames of the third order, is displayed. The image was decomposed into five scales where $\rho = 1.31$. Then, it was subjected to a repeated regularized processing with $\rho = 0.09$.

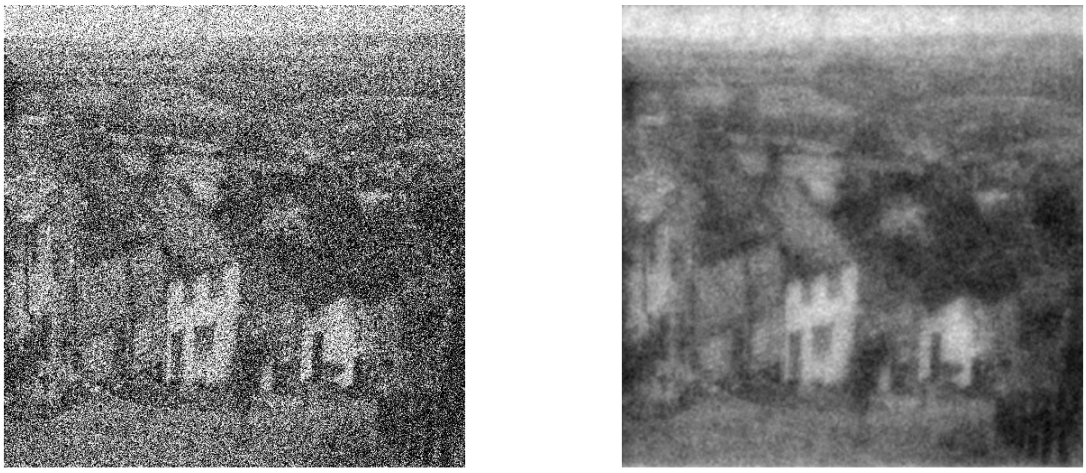

Figure 17: Left: Goldhill corrupted by a Gaussian noise with STD=100, PSNR=8.13. Right: The restored image, PSNR=23.06.

We display in Fig. 18 the Goldhill image corrupted by a Gaussian noise with STD=200, while PSNR=2.11. The image is buried almost completely in noise. In the right picture, the image is restored by the application of the regularized framelets derived from semi-tight frames of the fifth order. The image was decomposed into five scales, $\rho = 2.56$. Then, it was subjected to a repeated regularized processing with $\rho = 0.15$.

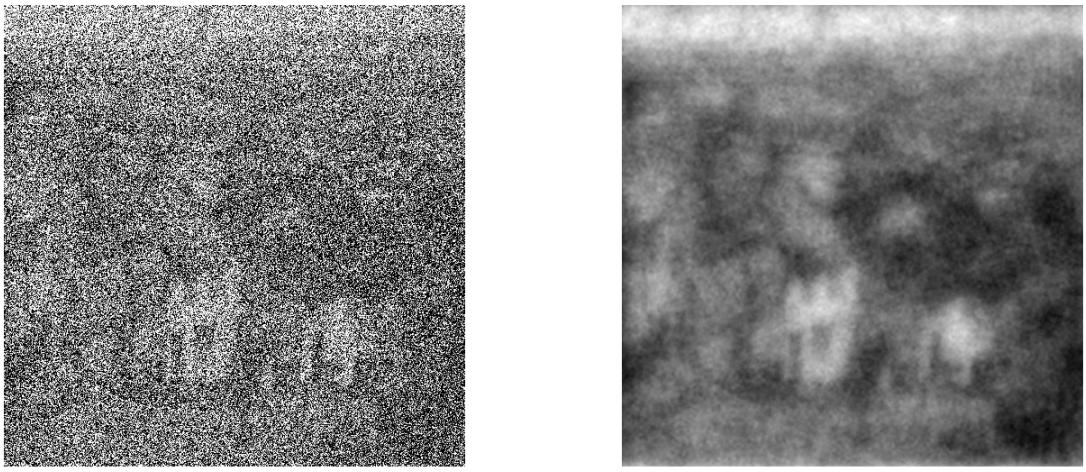

Figure 18: Left: Goldhill corrupted by a Gaussian noise with STD=200, PSNR=2.11. Right: The restored image, PSNR=21.41.

Fingerprint: We display in Fig. 19 the Fingerprint image corrupted by a Gaussian noise with

STD=300, while PSNR=-1.4. In the right picture, the image, which was restored by the application of the regularized framelets derived from semi-tight frames of the third order, is displayed. The image was decomposed into five scales, $\rho = 2.69$.

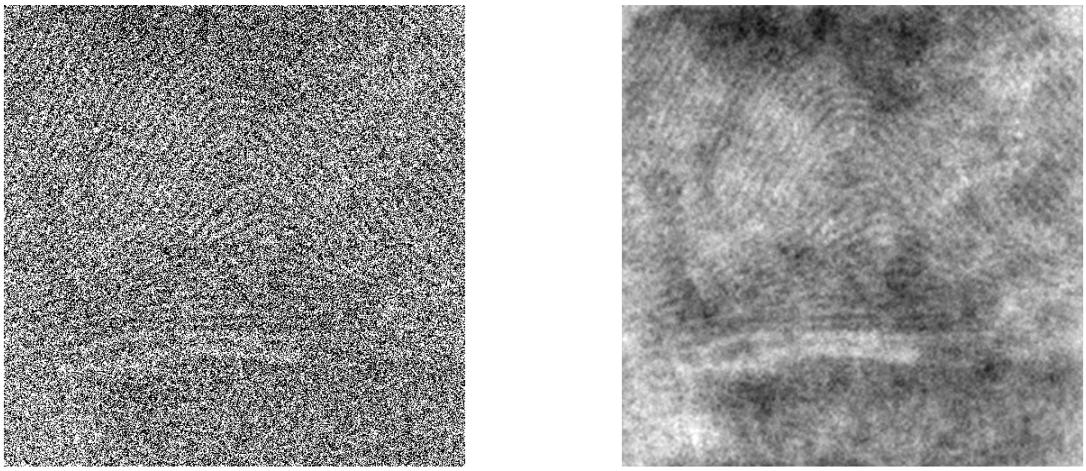

Figure 19: Left: Fingerprint corrupted by a Gaussian noise with STD=300, PSNR=-1.4. Right: The restored image, PSNR=16.1.

5 Discussion

We present an efficient algorithm for the restoration of images from highly noised originals. The algorithm is based on diverse library of tight and semi-tight wavelet frames. Unlike majority of current denoising methods, which threshold the transform coefficients, our algorithm performs direct and inverse multiscale transforms using properly modified frame filters. No thresholding is applied. The processing is linear. The algorithm is fast and can be implemented in real time. It depends on one numerical parameter ρ, which is estimated from the noise level. But, due to the high speed of the implementation, the parameter can be tuned manually, observing the results of the restoration with different ρ.

When a method that is based on thresholding is applied to a strongly noised image, then many transform coefficients are discarded. This results in either oversmoothing the output or in introduction of visual artifacts. Frequently, both phenomena are present. Our RF algorithm is free from these drawbacks. We compared our results with the results that were obtained by the application of the GSM method, which is considered to be one of most efficient and successful algorithm. Typically, the GSM-restored images have higher PSNR compared to RF-restored images. But these former images have visual artifacts, oversmoothed texture regions and some edges are distorted or eliminated. This

is not the case with the output from the application of our RF algorithm. The cost of implementation of the RF algorithm is much less than the implementation cost of the GSM method.

The diversity of available tight and semi-tight Butterworth frames provides an additional flexibility to the RF algorithm. It turned out that in most cases the regularized transforms, which were derived from semi-tight frames, outperform the transforms that were derived from tight frames. It happened because of the increased number of QVM in the analysis band-pass filters. In many examples, the regularized transform, which was derived from semi-tight frame of the fifth order, achieved the best performance. In this transform, the high-pass filter has ten QVM, the analysis band-pass filter has six QVM and the synthesis band-pass filter has four QVM.

References

[1] A. B. Pevnyi A. Z. Averbuch and V. A. Zheludev. Biorthogonal butterworth wavelets derived from discrete interpolatory splines. *IEEE Trans. on Sign. Proc.*, 49:2682–2692, 2001.

[2] A. Z. Averbuch, V. A. Zheludev, and T. Cohen. Interpolatory frames in signal space. *IEEE Trans. Sign. Proc.*, 54(6):2126–2139, June 2006.

[3] R. Coifman and D. Donoho. Translation-invariant de-noising. In *Wavelets and Statistics, A. Antoniadis and G. Oppenheim, Eds.*, pages 125–150, Berlin, Germany: Springer-Verlag, 1995.

[4] D. Donoho and I. Johnstone. Adaptating to unknown smoothness via wavelet shrinkage. *J. Amer. Stat. Soc.*, 90/432:1200–1224, 1994.

[5] D. Donoho and I. Johnstone. Ideal spatial adaptation via wavelet shrinkage. *Biometrica*, 81:425–455, 1994.

[6] E. D. Kolaczyk H. A. Chipman and R. M. McCulloch. Adaptive bayesian wavelet shrinkage. *J. Amer. Statist. Assoc.*, 92(440):1413–1421, 1997.

[7] M. Wainwright J. Portilla, V. Strela and E. Simoncelli. Image denoising using scale mixtures of gaussians in the wavelet domain. *IEEE Trans. Image Proc.*, 12:1338–1351, November 2003.

[8] I. A. Kakadiaris I. Konstantinidis D. Kouri L. Shen, M. Papadakis and D. Hoffman. Image denoising using a tight frame. *IEEE Trans. Image Proc.*, 15:1254–1263, May 2006.

[9] X. Li and M. Orchard. Spatially adaptive denoising under overcomplete expansion. In *Proc. Int. Conf. Image Processing, vol. 3*, pages 300–303, Vancouver, BC, Canada, September 2000.

[10] A. V. Oppenheim and R. W. Schafer. *Discrete-time signal processing.* Englewood Cliffs, New York, Prentice Hall, 1989.

[11] B. Yu S. G. Chang and M. Vetterli. Adaptive wavelet thresholding for image denoising and compression. *IEEE Trans. on Image Proc.*, 9:1532–1546, 2000.

[12] L. Şendur and I. W. Selesnick. Bivariate shrinkage functions for wavelet-based denoising exploiting interscale dependency. *IEEE Trans. on Sign. Proc.*, 50:2744–2756, 2002.

[13] E. P. Simoncelli and E. H. Adelson. Noise removal via bayesian wavelet coring. In *Proc. 3rd Int. Conf. on Image Processing, vol. I*, pages 379–382, Lausanne, Switzerland, 1996.

[14] E. P. Simoncelli and W. T. Freeman. The steerable pyramid: A flexible architecture for multi-scale derivative computation. In *Proc 2nd IEEE Int. Conf. on Image Processing, vol. III*, pages 444–447, Washington, DC, 1995.

[15] A. N. Tikhonov and V. Y. Arsenin. *Solution of ill-posed problems.* Wiley, New York, 1977.